J Nanopart Res (2018) 20: 72
https://doi.org/10.1007/s11051-018-4166-x

RESEARCH PAPER

Synthesis and characterization of magnetite-maghemite nanoparticles obtained by the high-energy ball milling method

A. A. Velásquez · C. C. Marín · J. P. Urquijo

Received: 25 October 2017 / Accepted: 14 February 2018 / Published online: 13 March 2018

Abstract We present the process of synthesis and characterization of magnetite-maghemite nanoparticles by the ball milling method. The particles were synthesized in a planetary ball mill equipped with vials and balls of tempered steel, employing dry and wet conditions. For dry milling, we employed microstructured analytical-grade hematite (α-Fe_2O_3), while for wet milling, we mixed hematite and deionized water. Milling products were characterized by X-ray diffraction, transmission electron microscopy, room temperature Mössbauer spectroscopy, vibrating sample magnetometry, and atomic absorption spectroscopy. The Mössbauer spectrum of the dry milling product was well fitted with two sextets of hematite, while the spectrum of the wet milling product was well fitted with three sextets of spinel phase. X-ray measurements confirmed the phases identified by Mössbauer spectroscopy in both milling conditions and a reduction in the crystallinity of the dry milling product. TEM measurements showed that the products of dry milling for 100 h and wet milling for 24 h consist of aggregates of nanoparticles distributed in size, with mean particle size of 10 and 15 nm, respectively. Magnetization measurements of the wet milling product showed little coercivity and a saturation magnetization around 69 emu g^{-1}, characteristic of a nano-spinel system. Atomic absorption measurements showed that the chromium contamination in the wet milling product is approximately two orders of magnitude greater than that found in the dry milling product for 24 h, indicating that the material of the milling bodies, liberated more widely in wet conditions, plays an important role in the conversion hematite-spinel phase.

Keywords Ball milling · Hematite to magnetite-maghemite conversion · Nanoparticles · Mössbauer spectroscopy · Transmission electron microscopy · Synthesis by attrition

Electronic supplementary material The online version of this article (https://doi.org/10.1007/s11051-018-4166-x) contains supplementary material, which is available to authorized users.

A. A. Velásquez (✉) · C. C. Marín
Grupo de Electromagnetismo Aplicado, Universidad EAFIT, A.A. 3300, Medellín, Colombia
e-mail: avelas26@eafit.edu.edu.co

C. C. Marín
e-mail: cmarina2@eafit.edu.edu.co

J. P. Urquijo
Grupo de Estado Sólido, Universidad de Antioquia, A.A. 1226, Medellín, Colombia
e-mail: jurquijo@udem.edu.co

Introduction

Iron oxides are a group of materials that have attracted increasing attention due to their broad range of applications, such as industrial pigments (Escobar et al. 2007), precursor for magnetic fluids, and precursor for thin films (Feng et al. 1975), among others. Magnetite (Fe_3O_4) and maghemite (γ-Fe_2O_3) are the most studied compounds because of their high magnetic response and

semiconducting behavior (Chiba et al. 2002). Different methods for synthesizing iron oxide particles have been reported in the literature, and among them are sol-gel (Chang et al. 1997), coprecipitation (Iwasaki et al. 2009), and hydrothermal (Morales et al. 2011) and solid-state reactions (Iwasaki et al. 2010; Chicinas 2006). Wet methods are a good alternative for obtaining crystalline particles with high magnetization; besides, they are low cost and little instrumentation is required. However, purely wet methods are not friendly with the environment and often, they require control of many variables, such as pH, addition rate of reagents, deaeration, agitation speed, and temperature, among others. In the search for other cleaner methods, high-energy ball milling turns out to be a good method to prepare nanoparticles of a variety of materials and alloys (Chicinas 2006) due to its simplicity, environmentally friendly, and its possibility of scaling to an industrial level.

In this work, we report a simple method for obtaining nanoparticles of the spinel system magnetite-maghemite by the ball milling technique, starting from microstructured analytical-grade hematite. For this purpose, we carried out two experiments, the first one employing only hematite as precursor material and the second one employing a mixture of hematite and deionized water. Milling conditions for both experiments were selected based on previous studies (Iwasaki et al. 2010; Chicinas 2006; Can et al. 2010; Kaczmarek and Ninham 1994; De Carvalho et al. 2013; Zdujic´ et al. 1999; Sahebary et al. 2009; Meillon et al. 1995; Globus et al. 1977; Randrianantoandro et al. 2001), where factors such as precursor materials, milling time, atmosphere, ball-to-powder mass ratio ($mass_{balls}/mass_{powder}$), and angular velocity of vials are pointed as determinant to activate the transformation hematite to magnetite-maghemite. The mechanism of conversion hematite to magnetite-maghemite by mechanosynthesis is still an object of study. To cite some works developed in this field, Zdujic´ et al. (1999) achieved complete conversion hematite-magnetite by dry milling in air atmosphere. They proposed a mechanism based on reduction of partial oxygen pressure generated during milling process, this process being favored by the high and rapid energy transfer from milling bodies to powder through continuous fracture and particle size reduction, which makes unstable the hematite phase and promotes the formation of magnetite as stable phase in that condition. Sahebary et al. (2009) have proposed a mechanism based on thermodynamic methods, where the energy transference from the grinding bodies to the milling material by amorphization and dislocations govern the transformation of hematite to magnetite at 325 K. Meillon et al. (1995) obtained sub-micrometric particles of maghemite through the method described by Globus et al. (1977); in this method, micrometric particles of hematite are comprised and sheared between two rubbing surfaces under constant flow of ethanol; the transformation of hematite-maghemite is observed after 55 days of milling, with 57% of maghemite and 43% of hematite in the product, these percentages being estimated from saturation magnetization measurements. Randrianantoandro et al. (2001) reported direct conversion of microstructured hematite to nanostructured maghemite by high-energy ball milling, starting from a mixture of hematite and ethanol, by using a ball-to-powder mass ratio of 110:1 and working to the maximum angular velocity of the mill (1460 rpm); ethanol was used as dispersing liquid to limit reduction of Fe^{3+} ions of hematite during its contact with the material of the milling bodies as well as prevent aggregation of the particles in the final products. The authors point the shearing effect on the crystalline grains of hematite during ball milling as the main mechanism to drive the transformation.

Taking into account this background, our intention with these experiments is to corroborate the possibility of producing nanostructured magnetite-maghemite particles starting from microstructured hematite, by using simplified milling conditions, where a reasonable milling time and a low weathering of the mill allow obtaining an efficient transformation of the precursor material to the spinel system, the foregoing looking to contribute to standardize synthesis methods of magnetic materials for technological applications, without the need to make much experiments.

Materials and methods

Mechanosynthesis experiments were performed with a planetary ball mill FRITSCH, model Pulverisette 7 premium line. Two hardened steel vials, 80 cm^3 volume, charged with 60 hardened steel balls 3 mm in nominal diameter, were used as the milling bodies. In both mills, 2.0 g of analytical-grade hematite (α-Fe_2O_3) with particle size around 0.5 μm, supplied by Sigma-Aldrich, was used as the precursor material. In the wet milling, 5 ml of deionized water was added to the hematite precursor.

In both mills, the angular velocity of the mill was programmed to 200 rpm, without atmosphere control. The milling time was 24 h in both cases and the vials were kept closed during all the experiments. The sample obtained by wet milling was placed in a drying oven Memmert UNE 400, at 60 °C for 24 h, in order to remove the residual water.

The identification of the phases and the structural analysis of the milling products were performed by X-ray diffraction, by using a diffractometer XPERT-PRO from PANalytical, operating at 45 kV, 40 mA, with Cu-K_α radiation ($\lambda = 1.540598$ Å) in the range of $2\theta = 10$–$80°$ and angular step of 0.0167°. Diffractograms were processed with the software Powder X (Dong 1999) in order to remove the continuous background signal of the tube and obtain the position of the peaks, the full width at half maximum of peak, the integral breadth, and the indexing of peaks. Morphology and particle size were analyzed with a transmission electron microscope Tecnai F20 Super Twin TMP, operating at 200 kV. The magnetic phases and hyperfine interactions in the magnetic nanoparticles were studied by transmission Mössbauer spectroscopy at room temperature, with a Mössbauer spectrometer developed in our laboratory (Velásquez et al. 2005), which operates in the constant acceleration mode, with a radioactive source of ^{57}Co(Rh), with initial activity of 25 mCi and velocities between − 12 and 12 mm/s. Thin absorbers with disk shape and effective thickness of 6 mg/cm^2 of iron were prepared for these measurements. Hysteresis loops at room temperature were obtained with a vibrating sample magnetometer developed in our laboratory, which has a resolution of 3×10^{-4} emu in magnetic moment and a range of 5 kOe in magnetic field. Traces of chromium coming from the milling bodies were analyzed with a UNICAM 929 AA spectrometer with chromium lamp; the samples were first solubilized in HCl solutions and then diluted in water to keep the chromium concentrations within the linear region of quantification.

Results

The milling products

Figure 1 shows a view of the milling materials, before and after milling. In the case of the dry milling, the final product presented a color change, passing from red in the precursor material to brown. In the case of the wet milling, the final product presented a crumb texture of black color. The sample recovered from the vial of the wet milling was put in a drying oven at 60 °C during 24 h to remove the residual water present.

X-ray diffraction measurements

Figure 2a–c shows the X-ray diffraction patterns of the precursor, dry milling product, and wet milling product, respectively. The peaks of the diffraction pattern of the precursor powder are consistent with those of hexagonal phase of hematite (National Bureau of Standards 1981). In the case of dry milling, presented in Fig. 2b, only peaks of the hexagonal phase of hematite were observed, which are wider and less intense than those of the precursor hematite. This pattern shows that dry milling reduces the crystallinity and/or the particle size of the precursor material, but it does not promote the transformation of hematite to magnetite or maghemite in our milling conditions. On the other hand, in the diffraction pattern of wet milling, presented in Fig. 2c, only peaks of spinel magnetite-maghemite system were identified, which points the important role of the water in the activation of the transformation hematite-spinel under mechanical milling.

Fig. 1 View of the milling materials. **a** Before and after dry milling. **b** Before and after wet milling

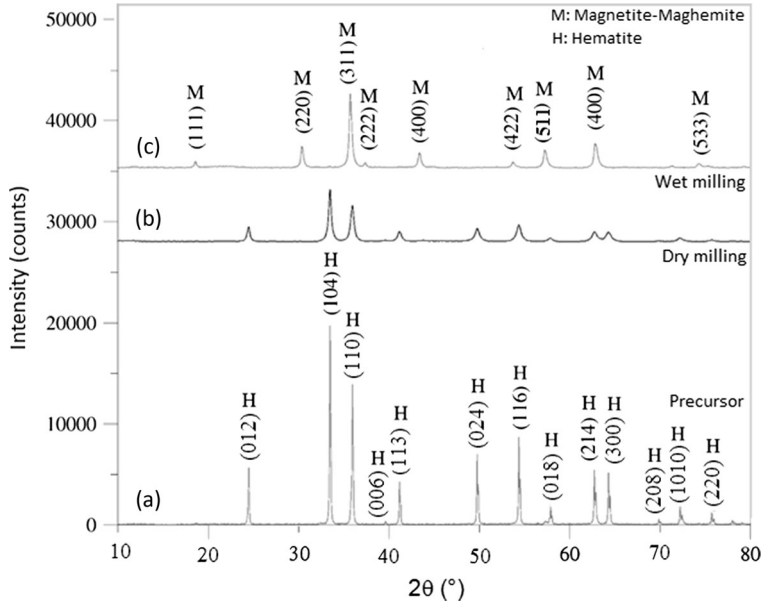

Fig. 2 X-ray diffraction patterns of the samples

Table 1 reports the parameters derived from the X-ray patterns; the mean crystallite diameter (D) was calculated from the method described by Monshi et al. (2012), where it is pointed out that the Cauchy-type profile gives less error than the Gaussian-type profile to estimate structural parameters. In a Cauchy-type profile, the broadening β of the peaks of the diffractogram is approximated by the contribution of two terms, namely,

$$\beta = \beta_m + \beta_n \tag{1}$$

The first term is the broadening resulting from the small crystallite size, given by

$$\beta_m = \frac{\lambda}{D cos\theta} \tag{2}$$

where

λ X-ray wavelength used (1.540598 Å)
D mean crystallite diameter

The second term is the broadening resulting from the lattice microstrain (β_n), given by

$$\beta_n = 4\varepsilon\, tan\theta \tag{3}$$

where ε is the lattice microstrain, defined as

$$\varepsilon = \frac{\Delta d}{d} \tag{4}$$

with d being the interplanar distance between (hkl) planes.

In all diffractograms, we calculated the broadening β as the integral breadth; this is the area under the peak divided by its maximum height (in radian). Because Eq. (1) involves the unknowns D and ε, two equations are necessary to solve both parameters. In our case, we selected two peaks without overlap in each diffractogram, located at angles $2\theta_1$ and $2\theta_2$, with $2\theta_1$ being the angle of the most intense peak. Afterward, we applied Eq. (1) in each angle and solved the system of two equations to obtain

$$D = \frac{\lambda(sin\theta_2 - sin\theta_1)}{\beta_1 sin\theta_2 cos\theta_1 - \beta_2 sin\theta_1 cos\theta_2} \tag{5}$$

$$\varepsilon = \frac{\beta_1 D cos\theta_1 - \lambda}{4D sin\theta_1} \tag{6}$$

The application of Eqs. (5) and (6) to the diffractogram of the precursor hematite gave negative values for D and ε, suggesting the absence of effects of microstrain in this sample. In this case, we applied the Scherrer equation to estimate the value of D, as follows:

$$D = \frac{K\lambda}{FWHM cos\theta} \tag{7}$$

Table 1 Diffraction and structural parameters derived from X-ray measurements

Sample	FWHM ($\times 10^{-3}$ rad)	$2\theta_1$ (°)	$2\theta_2$ (°)	β_1 ($\times 10^{-3}$ rad)	β_2 ($\times 10^{-3}$ rad)	I_{max} (counts)	D (nm)	ε	a (Å)	c (Å)
Precursor	1.5 ± 0.2	33.48 ± 0.01	35.95 ± 0.01	3.27 ± 0.02	4.02 ± 0.02	21,314	96 ± 13	–	5.035 (2)	13.754 (2)
Dry milling	4.7 ± 0.2	33.45 ± 0.01	35.94 ± 0.01	7.75 ± 0.04	7.98 ± 0.04	7210	30 ± 2	$2.0(4) \times 10^{-3}$	5.034 (2)	13.749 (2)
Wet milling	4.2 ± 0.2	35.72 ± 0.01	43.39 ± 0.01	6.59 ± 0.03	7.20 ± 0.04	9043	35 ± 2	$1.5(3) \times 10^{-3}$	8.324 (2)	–

FWHM full width at half maximum of the main peak, $2\theta_1$ angular position of the main peak of the diffractogram, $2\theta_2$ angular position of a second peak of the diffractogram, β_1 Integral breadth at the angle $2\theta_1$, β_2 integral breadth at the angle $2\theta_2$, I_{max} intensity of the main peak of the diffractogram, D mean crystallite diameter, ε microstrain, a, c Lattice parameter

where the Scherrer constant was taken as $K = 0.9$ and FWHM is the full width at half maximum of the main peak. The calculation of the uncertainties in the parameters D and ε is described in the supplementary material.

From the table, it is notable the increasing of both FWHM and β of the main peak in the diffraction pattern of the precursor hematite, as well as the decreasing of its maximum intensity (I_{max}) during dry milling, indicating a reduction in the crystallinity and/or particle size of the precursor, effect consistent with the milling process, where continuous fracture and defect propagation processes take place (Sahebary et al. 2009).

The lattice parameter of a crystalline magnetite (Fe_3O_4) is around 8.39 Å while the mean lattice parameter derived from the X-ray diffractogram is around 8.32 Å, a value closer to that of maghemite (γ-Fe_2O_3), around 8.35 Å (Randrianantoandro et al. 2001), indicating that wet milling process with the conditions here employed promotes the formation of a spinel system composed by a mixture of magnetite and maghemite. As we will see in the "Mössbauer measurements" section, the Mössbauer spectrum of the wet milling product shows, in addition to the characteristic sextet of Fe^{3+} ions occupying tetrahedral and octahedral sites in the spinel system, a second sextet with isomer shift characteristic of $Fe^{2.5+}$ ions of magnetite, where thermally activated electrons perform a hopping current between Fe^{3+} and Fe^{2+} ions occupying neighboring octahedral sites, which confirms the coexistence of magnetite and maghemite in this sample.

TEM measurements

Figure 3 presents the TEM micrographs of the samples. Particles of the precursor hematite, shown in Fig. 3a, present a hexagonal shape, with distributed sizes in the microscale. We do not have an image of the sample obtained during 24 h dry milling; however, Fig. 3b presents a micrograph of the sample obtained by dry milling for 100 h, where it is possible to observe that this consist of aggregates of nanoparticles. X-ray and Mössbauer spectroscopy measurements performed to this sample (not presented here for sake of brevity) did not evidence transformation of hematite to magnetite, indicating that the main effect of dry milling of hematite in air atmosphere is to reduce the crystallinity and particle size. Figure 3c, d presents two micrographs of the sample obtained by wet milling, where it is possible to observe some particles with sizes between 13 and

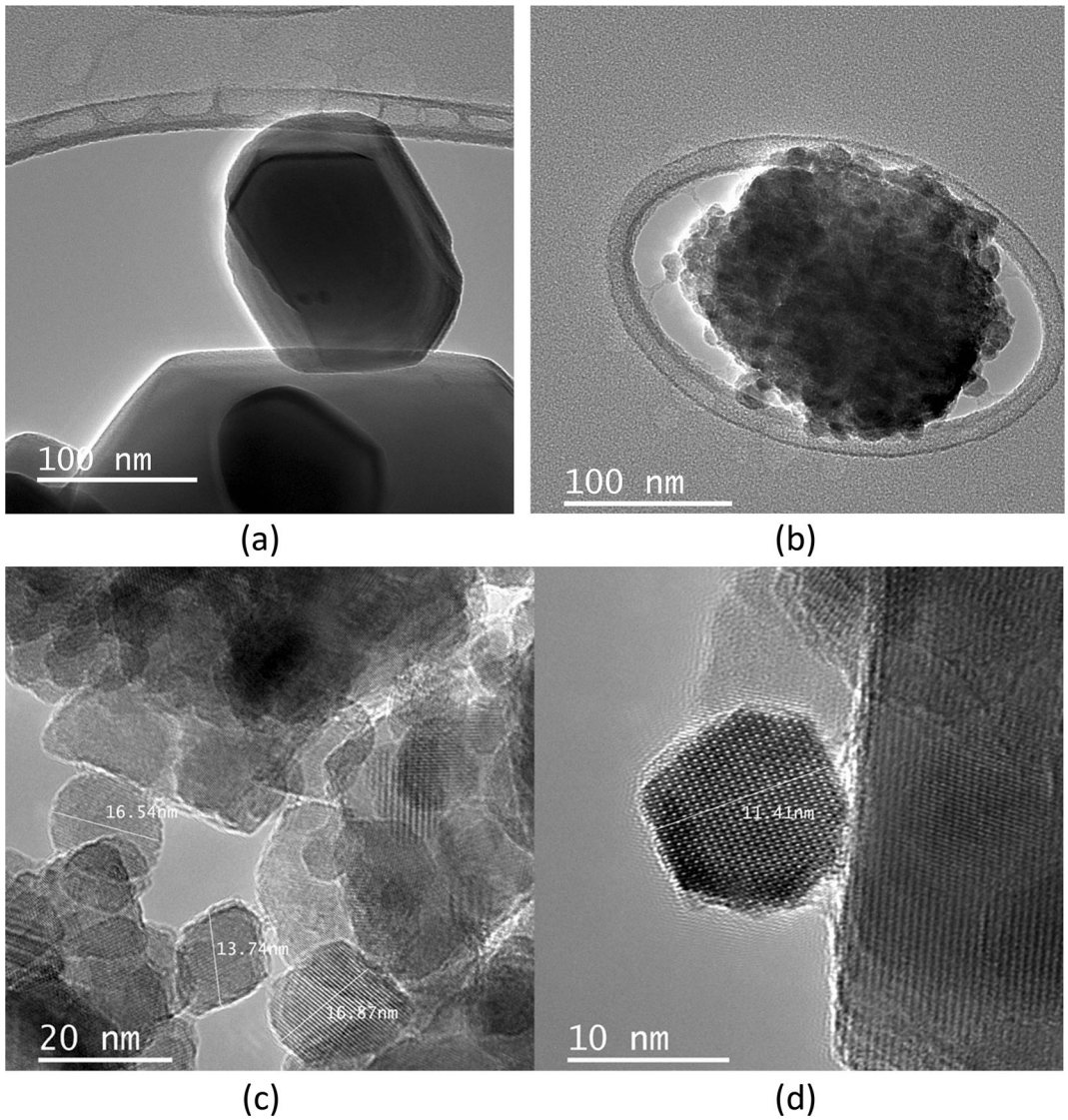

Fig. 3 TEM micrographs of the samples. **a** Precursor. **b** Dry milling for 100 h. **c**, **d** Wet milling

17 nm, as well as their crystalline planes, which assume a single orientation on the whole volume of the particles, indicating the formation of single-crystalline nanoparticles during wet milling.

Figure 4 shows the particle size histograms corresponding to the TEM micrographs presented in Fig. 3b, c. Both histograms were well described by distributions of log-normal type. The hematite nanoparticles distinguished in the sample obtained by dry milling for 100 h presented a mean particle size of 10 nm, with a standard deviation of 3 nm, while the spinel nanoparticles observed in the sample obtained by wet milling for 24 h presented a mean particle size of 15 nm, with a standard deviation of 11 nm. Although in the wet milling product the particles are aggregates, it is possible to recognize particles in the nanoscale, distributed in size, being 14 nm the most abundant size found in the micrographs. It is important to note that the mean crystallite size estimated by XRD in this sample is around twice the mean particle size estimated by TEM in the nanoparticles observed, which can be explained if one takes into account that the sample consists of particles very distributed in size, each composed of different crystallite volumes. The X-ray diffractogram gives account of the average crystallite size of the analyzed portion of the sample,

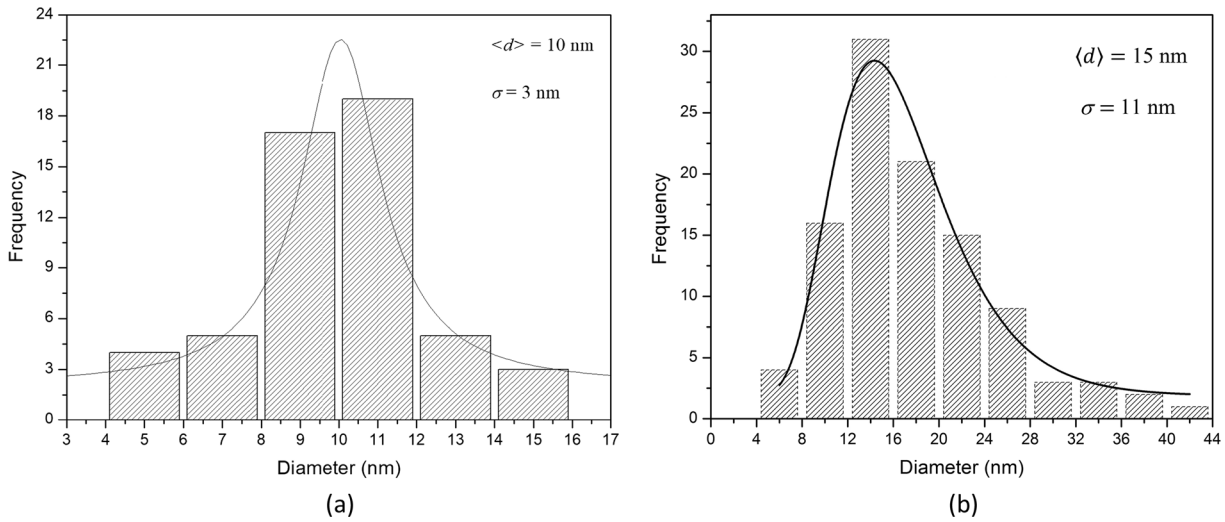

Fig. 4 Particle size distribution of the samples. **a** Dry milling for 100 h. **b** Wet milling

being this more representative of the overall sample than the local region analyzed by TEM.

Mössbauer measurements

Figure 5 presents the room temperature Mössbauer spectra of the samples, and Table 2 presents the hyperfine parameters derived from the fitting of the spectra with Lorentzian profile lines, by using the least square software MOSF (Vandenberghe et al. 1994). The spectrum of the precursor material shows a single sextet with hyperfine parameters characteristic of a crystalline and stoichiometric hematite (Vandenberghe 1990); on the other hand, the spectrum of the sample obtained by dry milling was well fitted with two sextets attributed to hematite but with different hyperfine magnetic fields. This spectrum presented peaks wider than that of the precursor hematite, indicating a reduction in the crystallinity and/or a wider particle size distribution during dry milling, this effect being consistent with the observations found in the X-ray pattern of this sample, where the diffraction peaks were widened and their intensity was reduced relative to the precursor sample. The fitting of this spectrum with two sextets can be explained from the partial reduction of the hyperfine magnetic field of the ^{57}Fe nuclei by the continuous mechanisms of fracture and amorphization occurring during the milling process, where particles with different sizes and degree of crystallinity are formed. The reduction in the crystallinity and particle size diminishes the hyperfine magnetic field in the ^{57}Fe nuclei because this interaction is sensitive to the environment of these nuclei via antiferromagnetic interactions with neighboring nuclei, this magnetic ordering being lower in less crystalline and smaller particles. Therefore, we attribute the sextet with hyperfine magnetic field of 51.6 T to those particles whose size and crystallinity are not significantly affected by milling, while the sextet with hyperfine magnetic field of 50.5 T is attributed to those particles whose size and crystallinity are significantly reduced by milling.

The spectrum of the sample obtained by wet milling was well fitted with three sextets, characteristic of a mixture of the phases of magnetite and maghemite. The sextets with hyperfine magnetic field of 49 T are attributed to Fe^{3+} ions of magnetite and Fe^{3+} ions of maghemite; on the other hand, the sextet with hyperfine magnetic field of 45.2 T is attributed to $Fe^{2.5+}$ ions occupying octahedral sites of magnetite, where hopping current between ions Fe^{2+} and Fe^{3+} occupying neighboring octahedra takes place. This contribution is attributed to the particles with largest sizes, where the inner ions Fe^{2+} do not reach to be oxidized.

The ratio $R = A(Fe^{2.5+})/A(Fe^{3+}) = 1.5(1)$ for the magnetite phase obtained by wet milling is lower than the value of 1.8 expected for a crystalline and stoichiometric magnetite (Vandenberghe 1990), which accounts for an overpopulation of Fe^{3+} in this sample that increases the spectral area $A(Fe^{3+})$ and therefore decreases the ratio R. The formation of maghemite can have two routes, the first one being the direct transformation of hematite to maghemite by mechanical activation during milling and the second one being the conversion of hematite to

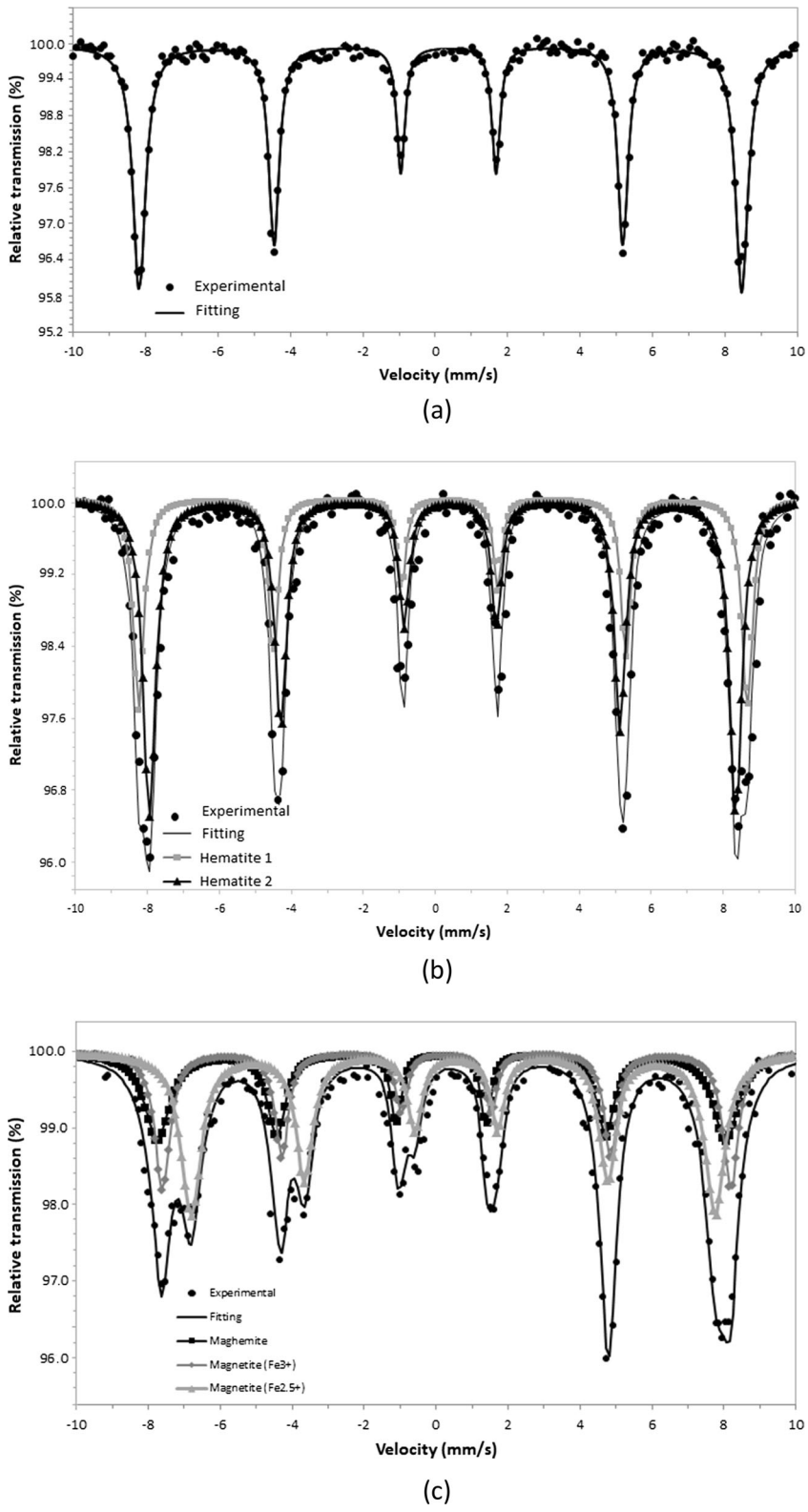

Fig. 5 Room temperature Mössbauer spectra of the samples. **a** Precursor hematite. **b** Dry milling. **c** Wet milling

Table 2 Mössbauer parameters of the iron phases identified in the milling products

Sample	Subspectrum	B_{hf} (T)	IS (mm s^{-1})	QS (mm s^{-1})	W (mm s^{-1})	A (%)
Precursor	Hematite	51.6 ± 0.2	0.36 ± 0.02	− 0.22 ± 0.02	0.27 ± 0.02	100
Dry milling	Hematite 1	51.6 ± 0.2	0.36 ± 0.02	− 0.19 ± 0.02	0.27 ± 0.02	36 ± 2
	Hematite 2	50.5 ± 0.2	0.37 ± 0.02	− 0.22 ± 0.02	0.35 ± 0.02	64 ± 2
Wet milling	Magnetite Fe^{3+}	49.0 ± 0.2	0.34 ± 0.02	0.01 ± 0.02	0.39 ± 0.02	28 ± 2
	Magnetite $Fe^{2.5+}$	45.2 ± 0.2	0.63 ± 0.02	− 0.08 ± 0.02	0.48 ± 0.02	43 ± 2
	Maghemite	49.0 ± 0.2	0.26 ± 0.02	0.01 ± 0.02	0.35 ± 0.02	29 ± 2

B_{hf} hyperfine magnetic field, *IS* isomer shift relative to α-Fe, *QS* quadrupole splitting, *W* line width of the innermost lines of each spectrum, *A* spectral area

magnetite by mechanical activation and the subsequent oxidation $Fe^{2+} \rightarrow Fe^{3+}$, as well as vacancy creation of Fe^{3+} in some particles of magnetite, giving place to the maghemite phase. The second route is expected to be more efficient in the smallest magnetite particles, due to their significant surface to volume ratio.

Magnetization measurements

Room temperature magnetization curves of the samples are presented in Fig. 6, and the main hysteresis parameters derived from the curves are presented in Table 3. Both, the precursor hematite and the hematite obtained by dry milling, present a low maximum magnetization, characteristic of antiferromagnetic phases; however, the maximum magnetization of the hematite with 24 h milling is reduced by 60% with respect to the maximum magnetization of precursor hematite, which is an indication of the effects of magnetic disorder produced by propagation of defects during the milling process.

It is also notable the increase by 123% of the coercive magnetic field of the dry milling sample with respect to the precursor sample, indicating a greater difficulty for the movement of the domain walls in the milled sample under reduction of the magnetic field. Again, this effect is consistent with the processes of fracture and defect propagation produced during ball milling, which increases the energy necessary for moving the domain walls (Özdemir and Dunlop 1997).

As can be observed in Fig. 6c, the magnetization of the sample obtained by wet milling does not reach the saturation state for magnetic fields less than 5 kOe. In order to estimate the saturation magnetization (M_s) of this sample, we fitted the magnetization curve with a ferromagnetic contribution of the type proposed by Beth and Cheng (1994), namely,

$$M(H) = \frac{2Ms^F}{\pi} \tan^{-1}\left[\frac{(H \pm H_c)}{H_c} \tan\left(\frac{\pi S}{2}\right)\right] \quad (8)$$

where M_s^F is the saturation magnetization of the ferromagnetic component of the sample, H_c is the coercive magnetic field, and S is the squareness of the hysteresis loop, defined as $S = M_r/M_S^F$. From the fitting curve, presented in Fig. 7, we obtained the following parameters: M_s^F = 69.4 emu g^{-1}, H_c = 148 Oe, and S = 0.14. According to this model, the spinel sample saturates approximately at H = 15 kOe (B = 1.5 T). The saturation magnetization is less than that expected for a crystalline and stoichiometric magnetite, around 92 emu g^{-1} (Can et al. 2010), but is higher than the saturation magnetization of a nanostructured maghemite, around 60 emu g^{-1} (Ramos et al. 2014), which supports the presence of both phases in the wet milling product. Although a Langevin model allows estimating the saturation magnetization of the sample by assuming non-interacting single-domain particles, the coercive field observed in the spinel sample indicates the presence of multidomain particles, which, according to TEM micrographs, are distributed in size. These particles do not exhibit a superparamagnetic behavior within the window time of measurement of Mössbauer spectroscopy of ^{57}Fe (10^{-8} s); this is due to the absence of doublets or very broaden lines in the spectrum. On the other hand, the hysteresis loop of the spinel system is very similar to that observed in sub-micrometric spinels synthesized by us in previous works (Morales et al. 2011), where magnetic saturation is observed for magnetic fields around

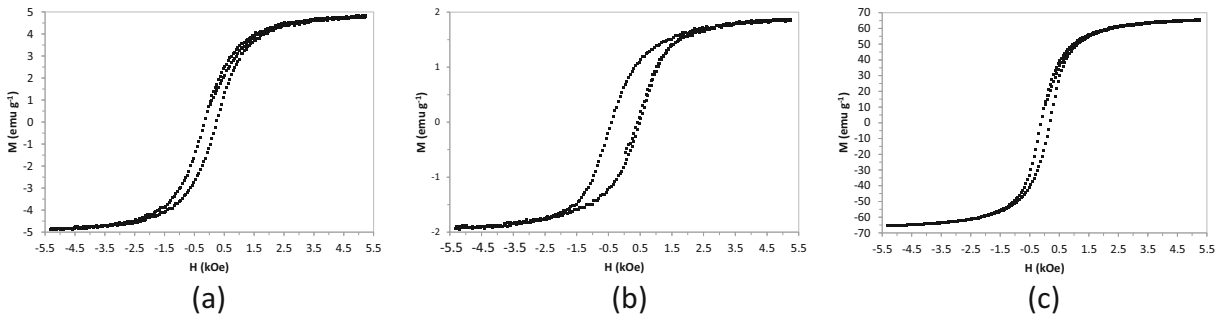

Fig. 6 Room temperature hysteresis loops of the samples. **a** Precursor hematite. **b** Dry milling. **c** Wet milling

1 T, which supports the use of a model based on ferromagnetic contribution.

Atomic absorption measurements

The vials and balls of the mill employed in our experiment are composed of tempered steel (FeCr). Table 4 shows the chromium traces found in the samples: dry milling for 24 h, dry milling for 100 h, and wet milling for 24 h. We did not analyze iron content because this element is the major component, both in the milling bodies as the precursor material, which does not allow us to separate the iron coming only from milling bodies.

From the table, it is important to observe that the chromium content found in the dry milling products increases with the milling time. On the other hand, it is possible to observe that the chromium content found in the sample obtained by wet milling is two orders of magnitude higher than that found in the sample obtained by dry milling for 24 h, indicating that deionized water promotes an important contribution of the material of the vial and the balls to the milling products. In particular, the iron present in the alloy FeCr of the milling bodies can play an important role in the transformation of hematite-spinel phase, via the contribution of Fe^{2+} to the products through production of ionic pairs FeO during the milling process.

Table 3 Hysteresis parameters of the samples

Sample	M_m (emu g^{-1})	M_r (emu g^{-1})	H_c (Oe)
Precursor	4.8 ± 0.1	0.9 ± 0.1	200 ± 2
Dry milling	1.9 ± 0.1	0.7 ± 0.1	446 ± 2
Wet milling	65.6 ± 0.2	13.3 ± 0.2	153 ± 2

M_m maximum magnetization reached in the experiment, M_r remanent magnetization, H_c coercive magnetic field

Possible mechanism of conversion of hematite-spinel phase

The mechanism of conversion of hematite to spinel phase by ball milling is very complex and controversial; however, we propose two possible routes for this transformation, which can occur simultaneously in our wet milling conditions in the presence of deionized water. As we have presented in the "The milling products," "X-ray diffraction measurements," "TEM measurements," "Mössbauer measurements," and "Magnetization measurements" sections, no spinel phase is formed in dry milling conditions, which is an indication of the important role of water in the transformation of α-Fe_2O_3 to Fe_3O_4 and γ-Fe_2O_3. Considering the liberation of material of the milling bodies to the products during the milling process, confirmed by atomic absorption spectroscopy, the first mechanism proposed suggest the obtaining of aqueous Fe^{2+} during reaction of the atmospheric oxygen inside the vial and that dissolved in the deionized water with the surfaces of the balls and the internal wall of the vial. This process is favored by the slightly acidic pH of deionized water employed (pH = 6.4), through the reaction

$$Fe_{(solid)} + \frac{1}{2}O_2 + 2H^+ \rightarrow Fe^{2+}_{(aqueous)} + H_2O \qquad (9)$$

Fe^{2+} ions solvated by water molecules can diffuse through the grains during collisions ball-powder-wall of the vial and ball-powder-ball. The diffusion of Fe^{2+} ions through the grains in the presence of the high energy provided by the constant mechanisms of fracture-coalescence occurring during milling favors the transformation from rhombohedral (hexagonal) to cubic

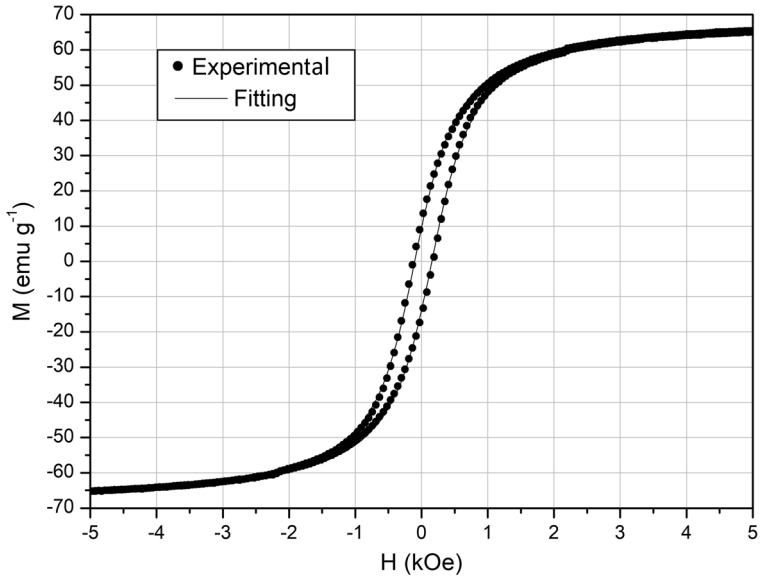

Fig. 7 Fitting of the hysteresis loop of the sample obtained by wet milling with a ferromagnetic contribution

phase. Those grains where no entrance of ions Fe^{2+} takes place give rise to the formation of maghemite.

The second mechanism proposed suggests an intermediate step occurring during wet milling process, consisting of the formation of wüstite (FeO) on the surface of the milling bodies, which is promoted by the reaction of these surfaces with the oxygen, both atmospheric inside the vial and dissolved in the deionized water. Ionic pairs of FeO can adhere superficially to the grains during collisions ball-powder-wall of the vial and ball-powder-ball, penetrating through the crystalline structure of these. Diffusion of ionic pairs of FeO through the grains in the presence of the high energy provided by the constant mechanisms of fracture-coalescence occurring during milling favors the conversion of hematite to magnetite, following the reaction

$$Fe_2O_3 + FeO \rightarrow Fe_3O_4 \quad (10)$$

Those grains where no entrance of ionic pairs FeO takes place give rise to the formation of maghemite.

Table 4 Chromium traces obtained by atomic absorption spectroscopy

Sample	Cr (μg/g)
Dry milling for 24 h	0.01255 ± 0.00001
Dry milling for 100 h	0.0350 ± 0.0002
Wet milling for 24 h	1.192 ± 0.006

By considering that formation of aqueous Fe^{2+} or FeO in wet milling is a non-controlled process, we do not expect to obtain a stoichiometric magnetite, which can support the value of the ratio $R = A(Fe^{2.5+})/A(Fe^{3+}) = 1.5(1)$ obtained for this phase in the Mössbauer measurements. It is very important to emphasize here that the formation of aqueous Fe^{2+} or FeO is promoted by the chemical composition of the vial and balls of our mill, which is rich in iron. This process has been reported in the literature (Štefanić et al. 2013, 2015), where the iron present in balls and vials of hardened steel is pointed as promoter of the formation of ferrous phases that react with the precursor material, this process not being observed in mills of other materials, such as tungsten carbide or corundum.

Conclusions

- Through the ball milling method, we have obtained nanostructured particles of the spinel system magnetite-maghemite, starting from a mixture of microstructured, analytical-grade hematite and deionized water.
- We have employed simplified milling conditions, where a complete conversion hematite-spinel system is obtained during 24 h milling, without an extreme power demand of the mill.
- With the milling parameters used in this work, the presence of water promotes the conversion of

hematite to spinel phase during the milling process. In absence of water, no conversion of hematite to spinel phases is observed for the same parameters used in the wet milling.

- The main effect observed in dry milling is a reduction in the crystallinity and particle size of the hematite particles.
- The presence of deionized water in the process and the iron liberated from the vial and balls of the mill can play an important role in the activation of the conversion of hematite to spinel system via generation of FeO ionic pairs.
- The magnetite phase obtained by wet milling is highly oxidized, which is evidenced by the value of the area ratio $R = A(Fe^{2.5+})/A(Fe^{3+})$ obtained in its Mössbauer spectrum, which is less than the value expected for a stoichiometric and crystalline magnetite.
- Further experiments are required to achieve milling parameters that allow obtaining particles less disperse in size; however, the wet milling conditions employed in our experiment are a good starting point for achieving this objective, considering the magnetic response, high conversion efficiency of hematite-spinel phase, and the scale of particle size obtained.

Compliance with ethical standards

Conflict of interest The authors declare that they have no conflict of interest.

References

Beth M, Cheng Y (1994) Determination of para-and ferromagnetic components of magnetization and magnetoresistance of granular Co/Ag films (invited). J Appl Phys 75:6894–6899

Can MM, Ozcan SC, Ceylan A, Firat T (2010) Effect of milling time on the synthesis of magnetite nanoparticles by wet milling. Mater Sci Eng B 172:72–75

Chang HSW, Chiou C, Chen Y, Sheen SR (1997) Synthesis, characterization, and magnetic properties of Fe3O4 thin films prepared via a sol–gel method. J Solid State Chem 128:87–92

Chiba M, Morio K, Koizumi Y (2002) Microstructure and magnetic properties of iron oxide thin films by solid reaction. J Magn Magn Mater 239:457–460

Chicinas I (2006) Soft magnetic nanocrystalline powders produced by mechanical alloying routes. J Optoelectron Adv Mater 8(2):439–448

De Carvalho JF, De Medeiros SN, Morales MA, Dantas AL, Carric AS (2013) Synthesis of magnetite nanoparticles by high energy ball milling. Appl Surf Sci 275: 84–87

Dong C (1999) Powder X: Windows-95-based program for powder X-ray diffraction data processing. J Appl Crystallogr 32: 168–173

Escobar DM, Arroyave C, Calderón J, Margarit I, Mattos O (2007) Paintings pigmented with doped magnetite: preliminary evaluation of anticorrosive properties. Revista de la Facultad de ingeniería Universidad de Antioquia 41:21–30

Feng JSY, Pashley RD, Nicolet M (1975) Magnetoelectric properties of magnetite thin films. J Phys C Solid State Phys 8: 1010–1022

Globus A, Pascard H, Cagan V (1977) Distance between magnetic ions and fundamental properties in ferrites. Journal de Physique, Colloque C1, supplément au N° 4, 38, C1-163

Iwasaki T, Kosaka K, Yabuuchi T, Watano S, Yanagida T, Kawai T (2009) Novel mechanochemical process for synthesis of magnetite nanoparticles using coprecipitation method. Adv Powder Technol 20(6):521–528

Iwasaki T, Kosaka K, Watano S, Yanagida T, Kawai T (2010) Novel environmentally friendly synthesis of superparamagnetic magnetite nanoparticles using mechanochemical effect. Mater Res Bull 45:481–485

Kaczmarek WA, Ninham BW (1994) Preparation of Fe3O4 and α-Fe2O3 powders by magnetomechanical activation of hematite. IEEE Trans Magn 30:732–734 Preparation of Fe/sub 3/O/sub 4/ and γ-Fe/sub 2/O/sub 3/ powders by magnetomechanical activation of hematite

Meillon S, Dammak H, Flavin E, Pascard H (1995) Existence of a direct phase transformation from hematite to maghemite. Philos Mag Lett 72(2):105–110

Monshi A, Foroughi MR, Monshi MR (2012) Modified Scherrer equation to estimate more accurately nano-crystallite size using XRD. World J Nano Sci Eng 2:154–160

Morales AL, Velásquez AA, Urquijo JP, Baggio E (2011) Synthesis and characterization of Cu^{2+} substituted magnetite. Hyperfine Interact 203:75–84

National Bureau of Standards (1981) Standard X-ray diffraction powder patterns. Lib Cong Catalog Card N: 53-61386, 37

Özdemir O, Dunlop DJ (1997) Effect of crystal defects and internal stress on the domain structure and magnetic properties of magnetite. J Geophys Res 102(B9):20211–20224

Ramos JA, Martínez AI, Osorio A, Valladares L, León L, Bustamante A (2014) Structural and magnetic properties of monophasic maghemite (γ-Fe2O3) nanocrystalline powder. Adv Nanoparticles 3:114–121

Randrianantoandro N, Mercier AM, Hervieu M, Greneche JM (2001) Direct phase transformation from hematite to maghemite during high energy ball milling. Mater Lett 47: 150–158

Sahebary M, Raygan S, Seyed SA, Abdizadeh H (2009) Inception of transformation of hematite to magnetite during mechanical activation: a thermodynamical approach. Iran J Sci Technol Trans B Eng 33(B5):415–424

Štefanić G, Krehula S, Štefanić I (2013) The high impact of a milling atmosphere on steel contamination. Chem Commun 49(81):9245–9247

Štefanić G, Krehula S, Štefanić I (2015) Phase development during high-energy ball-milling of zinc oxide and iron—the impact of grain size on the source and the degree of contamination. Dalton Trans 44(43):18870–18881

Vandenberghe RE (1990) Mössbauer spectroscopy and applications in geology. International training centre for post-graduate soil scientists. State University Gent, Belgium

Vandenberghe RE, De Grave E, De Bakker PMA (1994) On the methodology of the analysis of Mössbauer spectra. Hyperfine Interact 83:29–49

Velásquez AA, Trujillo JM, Morales AL, Tobón JE, Reyes L, Gancedo R (2005) Design and construction of an autonomous control system for Mössbauer spectrometry. Hyperfine Interact 161:139–145

Zdujić M, Jovalekić C, Karanović L, Mitrić M (1999) The ball milling induced transformation of α-Fe2O3 powder in air and oxygen atmosphere. Mater Sci Enf A 262:204–213 The ball milling induced transformation of α-Fe2O3 powder in air and oxygen atmosphere